A High-Precision Triangular Cylindrical Shell Finite Element

GARRY M. LINDBERG* AND MERVYN D. OLSON†
National Aeronautical Establishment, National Research Council, Ottawa, Canada

1.0 Introduction

RECENTLY, a highly successful refined triangular shallow shell element has been developed.[1] This element uses as generalized displacements the tangential displacements and their first derivatives, plus the normal displacement and its first and second derivatives at each vertex, a total of 36 in all. The transverse displacement function for the element contains a complete quartic polynomial plus some higher degree terms and allows a cubic variation of normal slope along each edge. The tangential displacement functions are complete cubic polynomials, and it is shown that this formulation leads to a consistent asymptotic strain energy convergence rate of n^{-6}, where n is the number of elements per side of a shell. Results show that this element is exceedingly accurate and far outperforms early lower order elements in predicting stresses as well as displacements.

This element may easily be converted into an efficient and useful cylindrical shell element simply by substituting cylindrical shell theory for the shallow shell theory. The purpose of this Note is to present the necessary derivations for doing this and to illustrate the element's usefulness on an example application. The problem of a cylindrical shell with a circular cut-out is analyzed, and the stress concentration results are compared with those from both an approximate analytic analysis[2] and a new finite difference variational approach.[3] The following presentation is necessarily brief, but more details are available in Ref. 4.

2.0 Cylindrical Shell Finite Element Formulation

The geometry for an arbitrary triangular cylindrical shell element is shown in Fig. 1. The strain energy of an isotropic

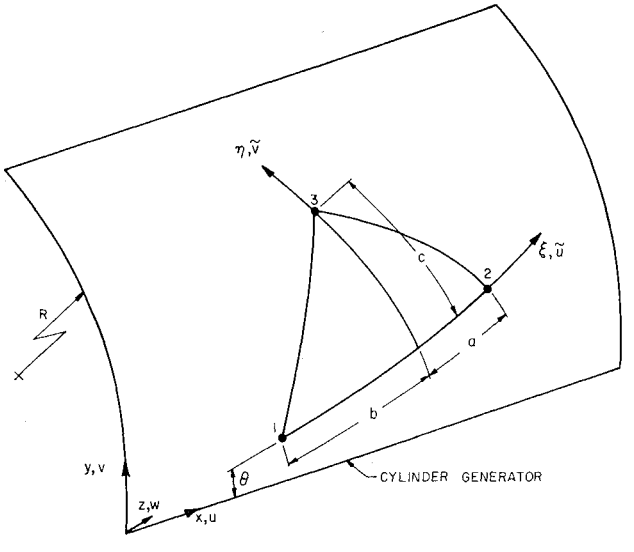

Fig. 1 Cylindrical shell triangular finite element geometry and coordinate systems.

Received August 12, 1970; revision received December 22, 1970.

* Associate Research Officer, Structures and Materials Laboratory. Member AIAA.

† Assistant Research Officer, Structures and Materials Laboratory; presently Assistant Professor, Department of Civil Engineering, University of British Columbia, Vancouver, Canada. Member AIAA.

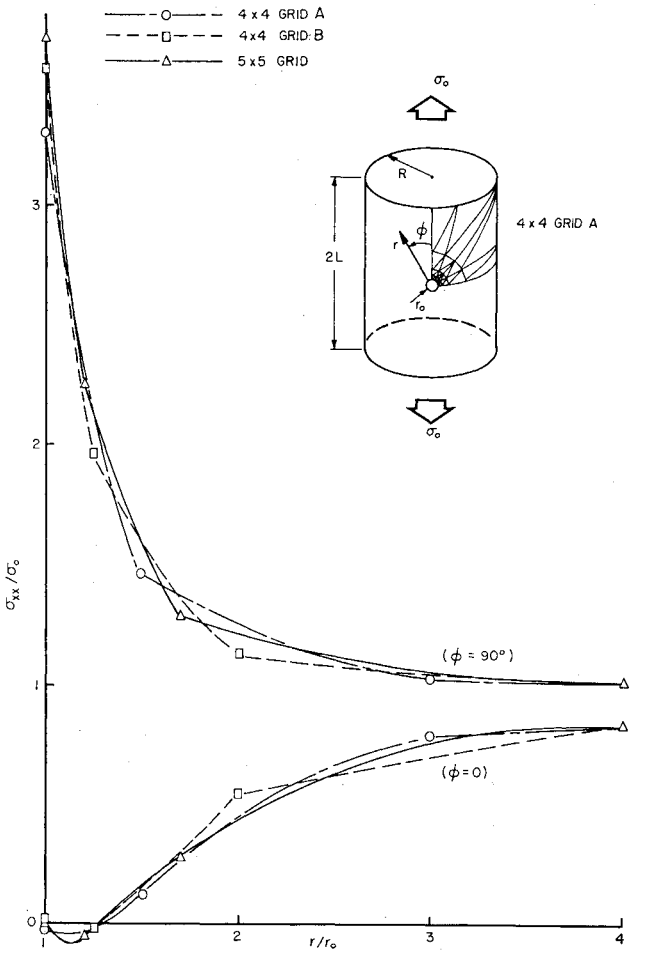

Fig. 2 Finite element predictions of σ_{xx} membrane stress distributions.

thin cylindrical shell element in global coordinates as given in Ref. 5 may be put in the form

$$U = [Et/2(1-\nu^2)]\iint\{d\}^T[L]\{d\}dxdy \tag{1}$$

where the column vector $\{d\}$ is

$$\{d\}^T = (u_x,u_y,v_x,v_y,w,w_{xx},w_{xy},w_{yy}) \tag{2}$$

and the matrix $[L]$ is easily derived. Note that subscripts denote differentiation.

The transformation from local to global coordinates is

$$\{d\} = [R_4]\{\tilde{d}\} \tag{3}$$

where

$$\{\tilde{d}\}^T = (\tilde{u}_\xi,\tilde{u}_\eta,\tilde{v}_\xi,\tilde{v}_\eta,w,w_{\xi\xi},w_{\xi\eta},w_{\eta\eta}) \tag{4}$$

and the rotation matrix $[R_4]$ is easily derived. Hence using

Table 1 Results for cylindrical shell with circular hole

	Number of unknowns	σ_{xx}/σ_0 at $r = r_0$, $\phi = 90°$ Membrane	σ_{xx}/σ_0 at $r = r_0$, $\phi = 90°$ Membrane + bending	Strain energy for $\frac{1}{4}$ cylinder $\times 10^4$
4 × 4 grid A	238	3.304	3.833	4.728772
4 × 4 grid B	238	3.572	4.108	4.728568
5 × 5 grid	367	3.690	4.249	4.729269
Analytic solution, Ref. 2		3.658	4.180	
Finite diff. solution, Ref. 3	753	3.603	4.096	
Strain energy for cylinder with no hole				4.712389

Eq. (3), the strain energy may be written in terms of an integral over local coordinates as

$$U = [Et/2(1 - \nu^2)]\iint\{\tilde{d}\}^T[\tilde{L}]\{\tilde{d}\}d\xi d\eta \quad (5)$$

where

$$[\tilde{L}] = [R_4]^T[L][R_4] \quad (6)$$

The displacement functions used in the shallow shell element[1] are also used here to insure conformity and high accuracy. That is, $\tilde{u}$, $\tilde{v}$ and w are written

$$\tilde{u} = \sum_{i=1}^{10} a_i\xi^{m_i}\eta^{n_i}, \quad \tilde{v} = \sum_{i=11}^{20} a_i\xi^{p_i}\eta^{q_i}, \quad w = \sum_{i=21}^{40} a_i\xi^{r_i}\eta^{s_i} \quad (7)$$

where m_i, n_i, p_i, q_i, r_i and s_i are just integers.

The stiffness matrix for the element is obtained from a calculation of strain energy

$$U = [Et/2(1 - \nu^2)]\{A\}^T[k]\{A\} \quad (8)$$

where $\{A\}$ is a 40-column vector of the polynomial coefficients a_i. The entries of the stiffness matrix $[k]$ are again determined in closed form and are given in the Appendix.

A transformation matrix $[T_1]$ relating generalized displacements in local coordinates to the polynomial coefficients and a rotation matrix $[R]$ relating the generalized displacements in local and global co-ordinates are then derived to give

$$[K_2] = [R]^T[T_1]^T[k][T_1][R] \quad (9)$$

the 38 × 38 stiffness matrix relative to global coordinates. Lastly, a static condensation procedure is used to eliminate the centroidal displacements u_c and v_c yielding finally a 36 × 36 stiffness matrix in terms of the global generalized displacements $\{W\}$, where

$$\{W\}^T = (u_1,u_{x1},u_{y1},v_1,v_{x1},v_{y1}, \times$$
$$w_1,w_{x1},w_{y1},w_{xx1},w_{xy1},w_{yy1},u_2\ldots,u_3\ldots) \quad (10)$$

The matrices $[T_1]$, $[R]$ and the condensation procedure are exactly the same as those used for the shallow shell element.[1] The resulting element is completely conforming and contains excellent approximations of all six required rigid body modes.

3.0 Example Application

To illustrate the accuracy of this element, the problem of a cylinder with a circular hole cut-out subjected to a uniform axial tensile stress at its free ends was solved. The physical parameters defining the problem were[3] $R = 10.0$ in., $t = 0.1$ in., r_0 (radius of hole) $= 1.1002$ in., L (half length of shell) $= 30$ in., $\nu = 0.3$ and $E = 10^7$ psi.

The problem was solved with two 4 × 4 and a 5 × 5 grid of elements, and the predictions of maximum stress concentrations and strain energies are given in Table 1. Grid A(4 × 4) had spacings of $l_1 = r_0/2$, $l_2 = 3r_0/2$, $l_3 = (L - 3r_0)/3$, $l_4 = 2(L - 3r_0)/3$, while grid B had $l_1 = r_0/4$, $l_2 = 3r_0/4$, $l_3 = (L - 2r_0)/5$, $l_4 = 4(L - 2r_0)/5$ where the l's are the radial dimensions of successive triangular elements proceeding outward from the hole. Membrane stress distributions calculated from the elements' polynomials are given in Fig. 2. The circle, square and triangle symbols represent nodal values. The results of an approximate analytic solution by Eringen et al.[2] together with the results of a new finite difference-variational solution by Johnson[3] are also given in Table 1.

The present results converge rapidly and are slightly larger than the Eringen et al. results for the 5 × 5 grid case. The membrane stress distributions are fairly smooth and seem converged as well. It is seen that the 4 × 4 grid B gives results comparable with the finite difference results but involves only one third the problem size. Hence, it may be concluded that the present method is significantly more efficient than the finite difference method.

The effect of element spacing is interestingly illustrated by the 4 × 4 grids A and B results. Although the stress concentration predictions are higher for grid B, the strain energy prediction is slightly lower. This illustrates that a grid with many elements concentrated in a region of high gradients may give better local predictions at the expense of slightly poorer over-all results.

A similar cylinder problem has been solved by Key and Beisinger[6] using a shell of revolution, shear deformation, quadrilateral finite element. With a coarse gridwork (approximately 800 unknowns), they predicted stress concentrations about 8% low, and with a fine grid (approximately 2800 unknowns), about 0.5% low. The fact that the present method yields similar accuracy with about an order of magnitude less equations reflects the current advancement in the state-of-the-art.

Appendix

$$\begin{aligned}
k_{ij} = {} & \tilde{L}(1,1)m_im_jF(m_i + m_j - 2,n_i + n_j) + \tilde{L}(1,2)[m_in_j + m_jn_i]F(m_i + m_j - 1,n_i + n_j - 1) \\
j \geq i + {} & \tilde{L}(1,3)m_ip_jF(m_i + p_j - 2,n_i + q_j) + \tilde{L}(1,4)m_iq_jF(m_i + p_j - 1,n_i + q_j - 1) + \\
& \tilde{L}(2,2)n_in_jF(m_i + m_j,n_i + n_j - 2) + \tilde{L}(2,3)n_ip_jF(m_i + p_j - 1,n_i + q_j - 1) + \\
& \tilde{L}(2,4)n_iq_jF(m_i + p_j,n_i + q_j - 2) + \tilde{L}(3,3)p_ip_jF(p_i + p_j - 2,q_i + q_j) + \\
& \tilde{L}(3,4)[p_iq_j + p_jq_i]F(p_i + p_j - 1,q_i + q_j - 1) + \tilde{L}(4,4)q_iq_jF(p_i + p_j,q_i + q_j - 2) + \\
& \tilde{L}(1,5)m_iF(m_i + r_j - 1,n_i + s_j) + \tilde{L}(2,5)n_iF(m_i + r_j,n_i + s_j - 1) + \\
& \tilde{L}(3,5)p_iF(p_i + r_j - 1,q_i + s_j) + \tilde{L}(4\,5)q_iF(p_i + r_j,q_i + s_j - 1) + \\
& r_j(r_j - 1)\{\tilde{L}(1,6)m_iF(m_i + r_j - 3,n_i + s_j) + \tilde{L}(2,6)n_iF(m_i + r_j - 2,n_i + s_j - 1) + \\
& \tilde{L}(3,6)p_iF(p_i + r_j - 3,q_i + s_j) + \tilde{L}(4,6)q_iF(p_i + r_j - 2,q_i + s_j - 1)\} + \\
& r_js_j\{\tilde{L}(1,7)m_iF(m_i + r_j - 2,n_i + s_j - 1) + \tilde{L}(2,7)n_iF(m_i + r_j - 1,n_i + s_j - 2) + \\
& \tilde{L}(3,7)p_iF(p_i + r_j - 2,q_i + s_j - 1) + \tilde{L}(4,7)q_iF(p_i + r_j - 1,q_i + s_j - 2)\} + \\
& s_j(s_j - 1)\{\tilde{L}(1,8)m_iF(m_i + r_j - 1,n_i + s_j - 2) + \tilde{L}(2,8)n_iF(m_i + r_j\,n_i + s_j - 3) + \\
& \tilde{L}(3,8)p_iF(p_i + r_j - 1,q_i + s_j - 2) + \tilde{L}(4,8)q_iF(p_i + r_j,q_i + s_j - 3)\} + \\
& \tilde{L}(5,5)F(r_i + r_j,s_i + s_j) + \tilde{L}(6,6)r_ir_j(r_i - 1)(r_j - 1)F(r_i + r_j - 4,s_i + s_j) + \\
& \tilde{L}(6,8)[r_is_j(r_i - 1)(s_j - 1) + r_js_i(r_j - 1)(s_i - 1)]F(r_i + r_j - 2,s_i + s_j - 2) + \\
& \tilde{L}(7,7)r_ir_js_is_jF(r_i + r_j - 2,s_i + s_j - 2) + \tilde{L}(8,8)s_is_j(s_i - 1)(s_j - 1)F(r_i + r_j,s_i + s_i - 4) = k_{ji}
\end{aligned}$$

where

$$F(m,n) = c^{n+1}[a^{m+1} - (-b)^{m+1}]m!n!/(m + n + 2)!$$

References

[1] Cowper, G. R., Lindberg, G. M., and Olson, M. D., "A Shallow Shell Finite Element of Triangular Shape," *International Journal of Solids and Structures*, Vol. 6, Aug. 1970, pp. 1133–1156.

[2] Eringen, A. C., Naghdi, A. K., and Thiel, C. C., "State of Stress in a Circular Cylindrical Shell with a Circular Hole," Welding Research Council Bulletin 102, Jan., 1965, Welding Research Council, New York.

[3] Johnson, D. E., "A Difference-Based Variational Method for Shells," *International Journal of Solids and Structures*, Vol. 6, 1970, pp. 699–724.

[4] Lindberg, G. M. and Olson, M. D., "A High Precision Triangular Cylindrical Shell Finite Element," Memo. ST-127, July, 1970, National Aeronautical Establishment Structures and Materials Lab., Ottawa, Canada.

[5] Bogner, F. K., Fox, R. L., and Schmit, L. A., "A Cylindrical Shell Discrete Element," *AIAA Journal*, Vol. 5, 1967, pp. 745–750.

[6] Key, S. W. and Beisinger, Z. E., "The Analysis of Thin Shells with Transverse Shear Strains by the Finite Element Method," AFFDL-TR-68-150, *Proceedings of the 2nd Conference on Matrix Methods in Structural Mechanics*, Wright-Patterson Air Force Base, Ohio, Oct. 1968.

Analysis of a Combustion Instability Problem Using the Technique of Multiple Scales

C. E. MITCHELL*

Colorado State University, Fort Collins, Colo.

Nomenclature

a = dimensionless sound speed = $a^*/\bar{a}_i^*$
B = dimensionless transfer number = $\bar{T} - \tau/\Delta l$
C = quantity defined after Eq. (1)
C_p = average specific heat at constant volume of the combustion product gas
L^* = combustion chamber length
M = Mach number = $\bar{u}^*/\bar{a}_i^*$
N = dimensionless droplet number density = $N^*(\rho_l^*/\rho_i^*)(4\pi r_i^{*3}/3)$
p = dimensionless pressure = $p^*(\bar{p}_i^*)^{1/2}$
P = dimensionless period of oscillation = $P^*\bar{a}_i^*/L^*$
r = dimensionless droplet radius = $r^*/\bar{r}_i^*$
T = dimensionless temperature = $T^*/\bar{T}_i^*$
t = dimensionless time = $t^*\bar{a}_i^*/L^*$
u = dimensionless axial velocity = $u^*/\bar{a}_i^*$
w = dimensionless mass generation = $w^*/\bar{\rho}_{li}^*u_l^*$
x = dimensionless axial variable = x^*/L^*
y = dimensionless axial variable = x/η
γ = ratio of specific heats
Δl = dimensionless latent heat of vaporization = $\Delta l^*/C_p^*T_i^*$
δ = dimensionless time variable = $2t/P$
ϵ = amplitude parameter = $M_e^{1/2}$
η = dimensionless combustion zone length = η^*/L
λ = dimensionless thermal conductivity = $\lambda^*/\bar{\lambda}_i^*$
μ = dimensionless viscosity = $\mu^*/\bar{\mu}_i^*$
ρ = dimensionless density = $\rho^*/\bar{\rho}_i^*$
σ = dimensionless entropy difference = σ^*/C_p^*
τ = dimensionless droplet temperature = $\tau^*/\bar{T}_i^*$

Superscripts

$\bar{}$ = steady-state quantity
^{1} = unsteady quantity
* = dimensional quantity

Subscripts

i = quantity evaluated at the injector face
l = liquid or droplet variable
e = quantity evaluated at nozzle entrance

Received September 14, 1970; revision received December 14, 1970. This work has supported in part by NSF Grant GK-3124.

* Assistant Professor, Department of Mechanical Engineering.

Introduction

THIS Note presents a nonlinear analysis of combustion-driven longitudinal mode pressure oscillations in a liquid rocket combustor.

Mitchell, Crocco, and Sirignano[1] and Crocco and Mitchell[2] have presented nonlinear analyses of similar oscillations in rocket motors having combustion source terms represented by the heuristic sensitive time-lag model devised by Crocco.[3] These analyses relied on the use of the Poincaré-Lighthill strained coordinate technique for their success. The combustion model employed in the work described here is based on a mechanistic droplet vaporization rate controlled model of the type used, for example, by Priem[4] in his instability studies. For this model, in addition to the use of the simplest kind of coordinate stretching, the technique of multiple scale is also employed in order to effectively pursue the analysis of the oscillations. A general discussion of the technique of multiple scales has been given by Cole.[5] It is to be emphasized that the purpose of this presentation is to demonstrate the effectiveness of the technique of multiple scales in the analysis of a particular nonlinear instability problem using a mechanistic combustion model, rather than to present a solution of the problem of nonlinear instability in terms of results with immediate practical application.

Problem Formulation

The combustor under consideration is assumed to be characterized by one-dimensional flow processes and purely axial oscillations. Combustion is assumed to occur between $x = 0$ and $x = \eta$. η is a function of time if oscillations are present. In the combustion region, a two-phase flow consisting of liquid fuel droplets and a constant composition calorically perfect combustion product gas is assumed. No droplet drag forces are considered and, in consequence of this, the liquid droplet velocity u_l is a constant. In addition, the droplet size at injection is taken to be constant at all times. For $x > \eta$ only product gas is present.

The model adopted in order to predict the liquid droplet vaporization rate is the simple collapsed flame model for a droplet in an infinite field combined with an empirical correction term to account for convection. (For a discussion of this model see, for example, Ref. 4). Using this model, the following expression describing the rate of vaporization of the liquid droplets results:

$$D_l r/Dt = -C/r \tag{1}$$

where

$$C = \frac{\lambda_i^* L^*}{C_p^* \rho_L^* a_i^* \bar{r}_i^{*2}} [1 + 0.3Re^{1/3}\mathrm{Pr}^{1/2}] ln(1 + B)$$

$$D_l/Dt = \partial/\partial t + u_l(\partial/\partial x)$$

$$Re = 2r^*\rho^*|u_l^* - u^*|/\mu^*, \quad Pr = C_p^*\mu^*/\lambda^*$$

The conservation equations (mass, momentum, energy) describing the gasdynamic field are written down in the form used by Crocco and Mitchell.[2] The set of three nonlinear partial differential equations in terms of p, u, and σ that results must satisfy a zero velocity condition at the injector and a constant Mach number ("short nozzle," see Ref. 1) condition at the entrance to the nozzle. In addition, all solutions are required to be periodic in time.

Solution of the Equations

The power series approach used to solve the aforementioned set of partial differential equations follows in a general way